processes

MDPI

Article

Research on Self-Excited Inverter Rectification Method of Receiver in Wireless Power Transfer System

Suqi Liu [1,*], Xueying Yan [1], Gang Wang [1] and Yuping Liu [2]

[1] School of Mechanical and Electrical Engineering, Guilin University of Electronic Technology, No.1 Jinji Road, Guilin 541004, China; yy2024731@126.com (X.Y.); gangwangsut@hotmail.com (G.W.)
[2] School of Electronic Engineering and Automation, Guilin University of Electronic Technology, No.1 Jinji Road, Guilin 541004, China; liuyuping2024@126.com
* Correspondence: liusuqi2009@126.com

Abstract: To decrease the complexity and increase the efficiency of wireless power transfer (WPT) systems, this paper proposes a novel self-excited invert rectification method for the design of the invert rectifier of the receiver (Rx). The self-excited invert rectifier can perform the self-driving and soft-switching of the MOSFETs as well as the frequency-tracking function without a microcontroller. This allows us to greatly simplify the structure of the invert rectifier and increase the transfer efficiency (TE) of the WPT system. Firstly, a self-excited invert rectifier circuit is designed, and a self-excited invert rectification method is studied. Additionally, the power loss of the self-excited invert rectifier is analyzed. Finally, the self-excited invert rectifier of the WPT experimental system is designed. The self-excited invert rectification method is then verified. The key component parameters of the self-excited invert rectifier are provided and optimized. The TE of the WPT system that includes the self-excited invert rectifier is improved by more than 5% without a microcontroller. The self-excited invert rectifier of the Rx provides a practical solution for decreasing the complexity and increasing the TE of the WPT system.

Keywords: wireless power transfer; self-excited invert rectifier; rectification method; receiver

check for updates

Academic Editor: Nikolay Yu. Peskov

Received: 3 November 2024
Revised: 23 December 2024
Accepted: 30 December 2024
Published: 2 January 2025

Citation: Liu, S.; Yan, X.; Wang, G.; Liu, Y. Research on Self-Excited Inverter Rectification Method of Receiver in Wireless Power Transfer System. *Processes* **2025**, *13*, 89. https://doi.org/10.3390/pr13010089

Copyright: © 2025 by the authors. Licensee MDPI, Basel, Switzerland. This article is an open access article distributed under the terms and conditions of the Creative Commons Attribution (CC BY) license (https://creativecommons.org/licenses/by/4.0/).

1. Introduction

Tesla conducted a WPT experiment in the early 20th century [1]. WPT technology then made great progress [2,3]. In recent years, it has been widely used in many fields, including car mobile phones, electric vehicles, and mobile robots [4–6].

A WPT system typically contains AC power and a resonant system containing a transmitter (Tx), receiver (Rx), and rectifier [7]. The design of the rectifier is usually based on the full-bridge rectifier. The system has high efficiency. However, its structure is complex [8–10]. Ref. [11] introduced right-half-plane zeros into small-signal transfer functions to resolve the current source nature of the series–series compensation. They proposed adopting a different rectifier configuration for the system. A novel single-phase bidirectional ac–dc WPT topology is proposed in [12]. It allows the drawbacks of matrix-converter-based topologies to be overcome while retaining the advantages of single-stage topologies. A bidirectional WPT system, which can function in both forward and reverse modes, was proposed in [13]. Ref. [14] proposed the LCC-S type compensation topology because magnetically coupled WPT systems face a wide input voltage range and variable load in some specific application scenarios, resulting in variable output voltage. Ref. [7] proposed a novel full-bridge step density modulation for WPT systems based on the step density averaging principle, which can achieve full-range ZVS operation. Ref. [15]

proposed a new six-switch topology based on the full-bridge converter, which achieves the self-adaptation of a dynamic change in system parameters. According to the above references, full-bridge inverters are used to convert DC to AC with a microcontroller on the Tx side. Additionally, four rectifier diodes are usually used for full-bridge rectification on the Rx side.

However, in the WPT research community, self-excited inverters are usually used on the Tx side. Ref. [16] used a self-excited inverter to construct the inversion stage of the WPT system without a PWM generator and a microcontroller, which greatly simplified the hardware structure. In addition, soft-switching (SS) and automatic frequency tracking (FT) can be performed without requiring additional control strategies, which also reduces the complexity. Ref. [17] proposed a self-excited inverter to obtain high-frequency AC power, which reduced the complexity of their WPT system. Additionally, the output voltage of the parallel–series WPT system with a self-excited inverter is resistant to load changes. An improved self-excited resonant circuit was also provided using a fully controlled low-power switch instead of a diode; the SS performance was improved, the temperature of the switch tube was reduced by about 7 °C, and the TE was also improved by about 4% [18]. The principle of a self-excited push–pull oscillation circuit was analyzed [19]. In a WPT system with a self-excited converter, the influence mechanism of magnetic shielding on the TE was analyzed; the optimal shielding distance was obtained [20]. These references indicate that self-excited inverters have a lot of excellent characteristics, such as SS, FT, the constant voltage output, etc. Thus, a method of the invert rectifier of the Rx is proposed by using the method and characteristics of the self-excited inverter on the Tx side, which is used to convert AC to DC without a microcontroller.

In view of the aforementioned studies, this paper proposes a novel self-excited invert rectification method to design the invert rectifier of the Rx, in order to reduce the complexity and increase the transfer efficiency (TE) of the WPT system. The self-excited invert rectifier can perform the self-driving (SD) and SS of the MOSFETs as well as the FT function without a microcontroller. This greatly simplifies the structure of the invert rectifier, and increases the TE of the WPT system. Firstly, a self-excited invert rectifier circuit is designed, and a self-excited invert rectification method is studied. Additionally, the power loss of the self-excited invert rectifier is analyzed. Finally, the self-excited invert rectifier of the WPT experimental system is then designed. The self-excited invert rectification method is then verified. The key component parameters of the self-excited invert rectifier are provided and optimized. The TE of the WPT system, which includes the self-excited invert rectifier, is improved by more than 5% without requiring a microcontroller. The self-excited invert rectifier of the Rx provides a practical solution for reducing the complexity and increasing the TE of the WPT system. In contrast to the existing works, the contributions of this article are as follows:

(1) A self-excited invert rectification method is proposed and applied to design the invert rectifier of the Rx.
(2) The key component parameters of the self-excited invert rectifier are provided and optimized to improve the TE.

The remainder of this paper is organized as follows. Section 2 describes the self-excited invert rectifier circuit, and provides a brief analysis of the working principle of the self-excited invert rectifier. Section 3 gives the analysis of the power loss of the self-excited invert rectifier. Section 4 presents the experiment results. Finally, conclusions are drawn in Section 5.

2. Design of the Self-Excited Invert Rectifier Circuit

The self-excited invert rectifier consists of a circuit with a symmetric structure, which can perform the SD and SS of the MOSFETs as well as the FT function without a microcontroller and without requiring additional control strategies.

A diagram of the WPT system with the self-excited invert rectifier, which includes a Tx and an Rx, is shown in Figure 1. Q_1–Q_4 are the MOSFETs used as switching transistors in a full-bridge inverter, V_{dc} is the input power, L_1 and L_2 are the coils, C_1 and C_2 are the capacitors, M is the mutual inductance of L_1 and L_2, D_1 and D_2 are the fly-wheeling diodes, R_1–R_4 are the voltage divide resistors, D_3 and D_4 are the rectifier diodes, D_5 and D_6 are the Zener diodes which provide a stable voltage to protect the Q_5 and Q_6 MOSFETs used as switching transistors in the self-excited invert rectifier, C_3 is the filter capacitor, R_L is the load resistor, u_a, u_b, u_c, and u_d are the voltages of points a, b, c, and d, respectively, and u_{ab} is the voltage between points a and b. The parameters of the circuit of the WPT system are shown in Table 1.

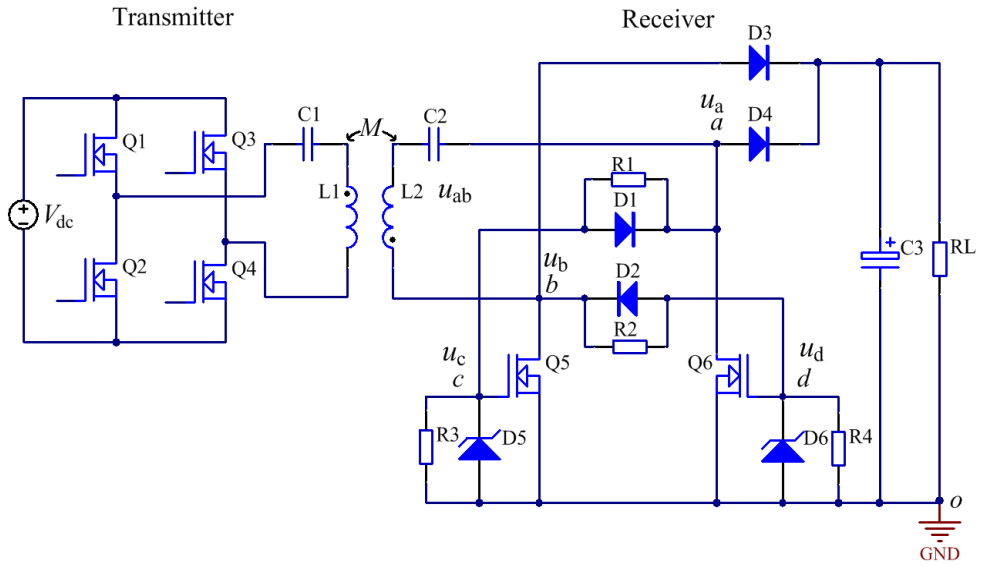


Figure 1. WPT system with self-excited invert rectifier.

Table 1. Parameters of the WPT system circuit with the self-excited invert rectifier.

Parameter	Value
V_{dc}	36 V
L_1 and L_2	15.0 μH
C_1 and C_2	294.6 nF
Q_1–Q_6	AGM035N10A is an N-channel MOSFET (drain-source on-state resistor: 3 mΩ)
R_1 and R_2	1 kΩ
R_3 and R_4	10 kΩ
D_1 and D_2	1N4148
D_3 and D_4	SB10100L (Vf: 670 mV@10 A)
D_5 and D_6	ZMM15
C_2	100 V, 100 μF

According to Figure 1 and Table 1, the self-excited invert rectifier part only includes D_1–D_6, R_1–R_4, Q_5, and Q_6. The self-excited invert rectifier with a few components can perform the self-driving and soft-switching of the MOSFETs as well as the frequency-tracking function without a microcontroller. This allows us to greatly simplify the structure of the invert rectifier and increase the TE of the WPT system.

In the Rx, the self-excited invert rectifier consists of a circuit with a symmetric structure. The wireless power is transferred from the Tx to the Rx through magnetic coupling resonance. Under high-frequency sine voltage stimulation on the Rx side, because of the existence of R_1–R_4, Q_5 and Q_6 cannot simultaneously be in a blocked state nor in a conducting state. This indicates that at any moment, one MOSFET is on and the other one is off. A brief analysis of the working principle of the self-excited invert rectifier is then provided. According to this working principle, the self-excited invert rectifier is divided into four working modes. The obtained results are shown in Figures 2–6. Assuming that at the beginning, Q_5 is turned on while Q_6 is blocked, the four working modes with $u_{ab} = -u_{ba}$, where Uth is the gate threshold voltage, are given as follows:

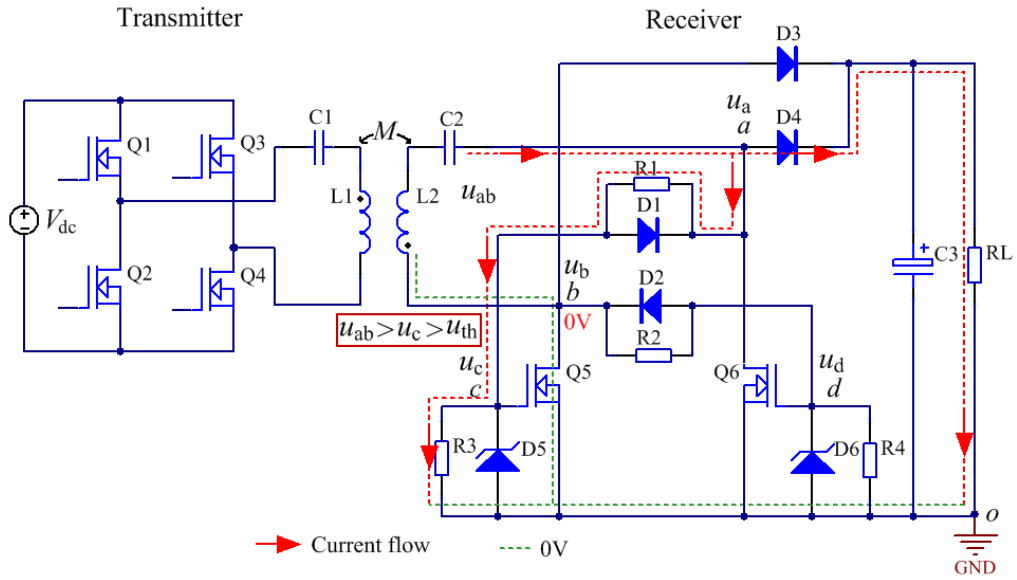


Figure 2. Working mode 1 of the self-excited invert rectifier: Current flow is power and control loops; and 0 V is the same voltage level.

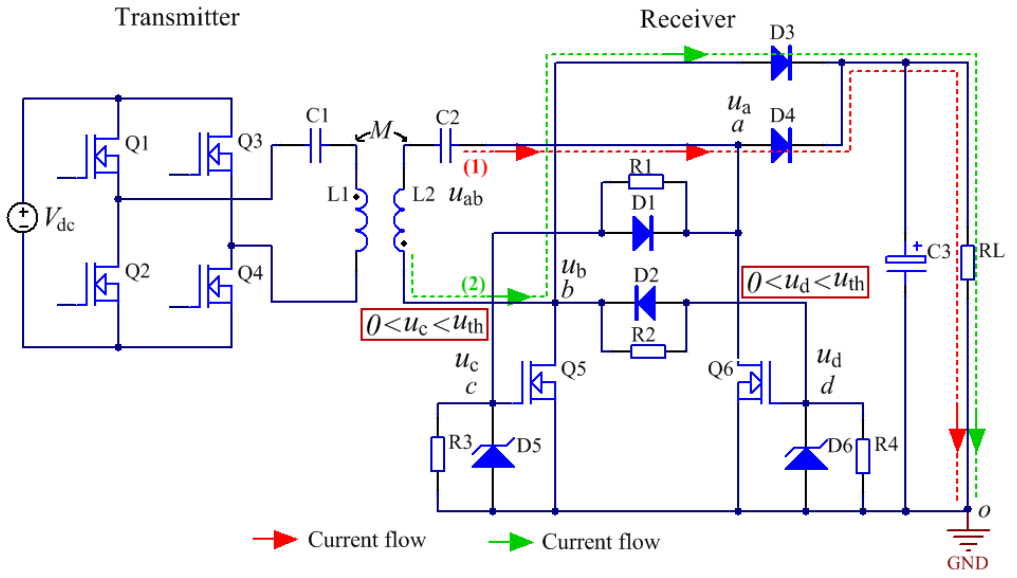


Figure 3. Working mode 2 of the self-excited invert rectifier: Current flow of red dotted lines is the first process section; and Current flow of green dotted lines is the second process section.

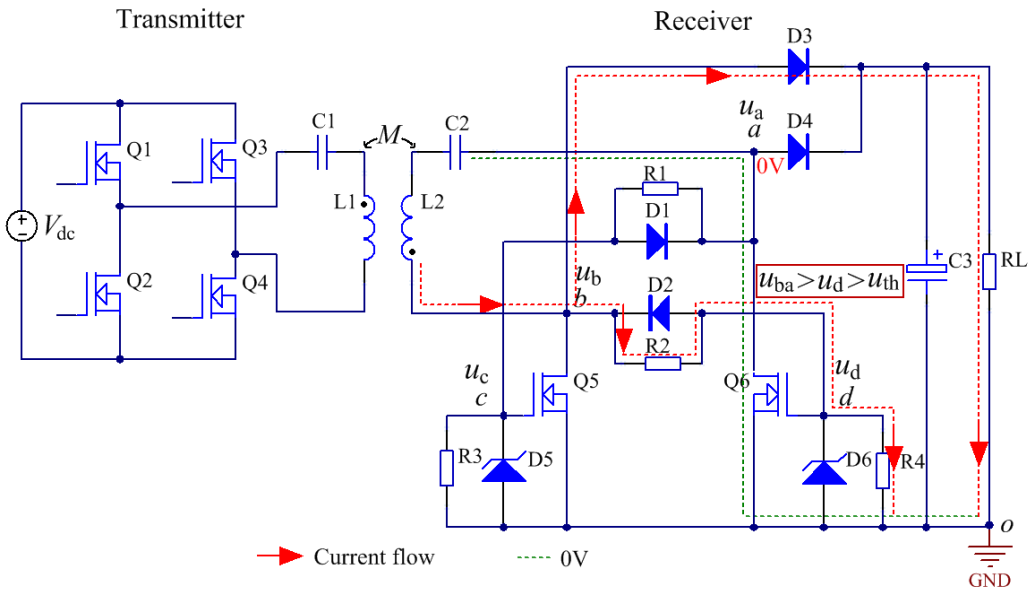


Figure 4. Working mode 3 of the self-excited invert rectifier: Current flow is power and control loops; and 0 V is the same voltage level.

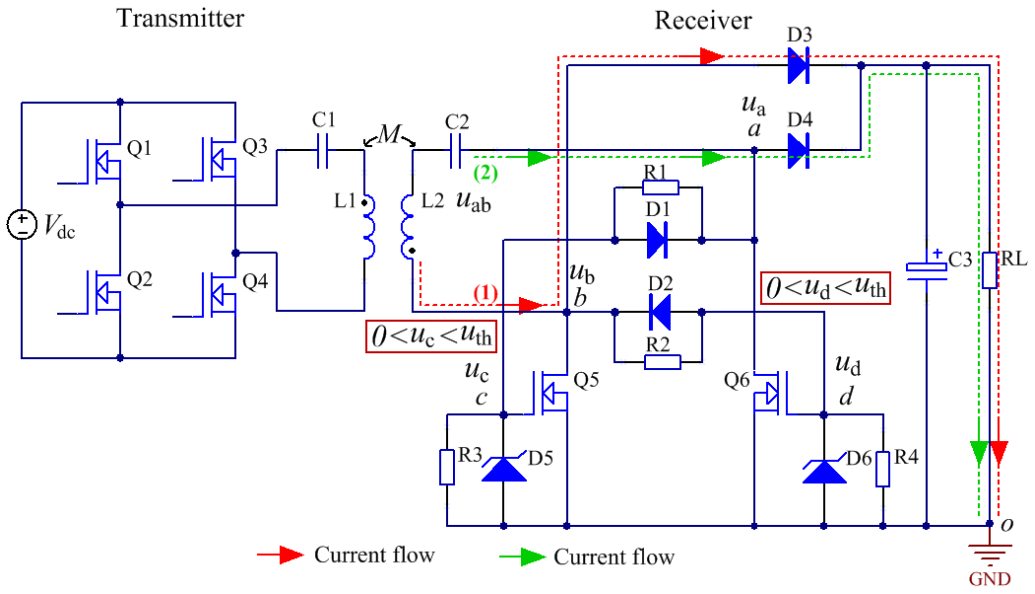


Figure 5. Working mode 4 of the self-excited invert rectifier: Current flow of red dotted lines is the first process section; and Current flow of green dotted lines is the second process section.

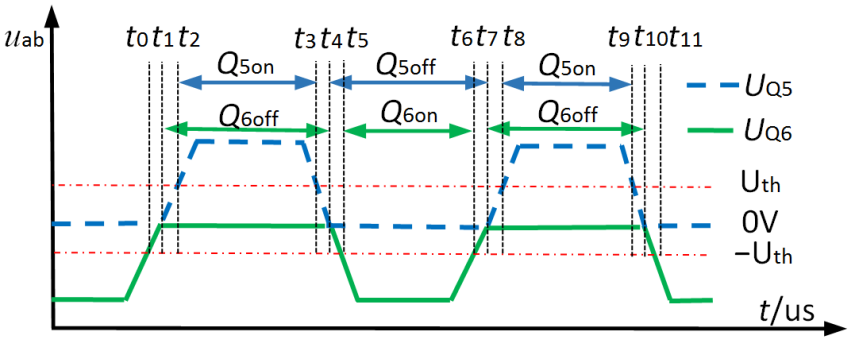


Figure 6. Steady−state working waveform of the switching tubes in the self-excited invert rectifier.

(1) Mode 1: Based on Figures 2 and 6, t_2 and t_3 are the on time of Q_5 (i.e., Q_{5on} time) and t_1–t_4 are the off time of Q_6 (i.e., Q_{6off} time). In other words, when u_{ab} increases from u_c = Uth to the peak and then decreases to u_c = Uth, Q_5 is turned on while Q_6 is blocked. The path of the current has two loops: power and control loops, (the red dotted lines in Figure 2). The power loop is from C_2, point a, D_4, and R_L to point *o*, while the control loop is from C_2, point a, R_1, point c, and R_3 to point *o*. Note that point *o*, Q_5, point b, and the bottom of L_2 have the same voltage level (0 V) (green dotted lines in Figure 2). In addition, R_1 and R_3 construct a voltage divider (VD) to provide bias voltage (BV) for Q_5. Similarly, R_2 and R_4 construct a VD to provide BV for Q_6. In this mode, Q_5 is turned on because $u_{ab} > u_c >$ Uth. On the contrary, Q_6 is blocked because $u_d = u_b = 0$ v. Thus, the invert rectifier circuit performs positive half-cycle rectification.

(2) Mode 2: According to Figures 3 and 6, when the high-frequency sine voltage u_{ab} decreases from u_c = Uth to zero, Q_5 enters the amplification region from the conductive one at t_3 and t_4. Q_5 is then blocked at time point t_4 and time regions t_4 and t_7. In addition, when Q_5 enters the amplification region and is blocked, the power is quickly released by a circuit loop of R_2 and D_2. This is the first process section (red dotted lines in Figure 3). On the other hand, the voltage is reversed at the next moment. When $u_{ba} = -u_{ab}$ increases from zero to u_d = Uth, Q_6 enters the amplification region at the time regions t_4 and t_5. Q_6 then turns on at the time point t_5 and the time regions t_5 and t_6 when u_{ba} increases and $u_d >$ Uth. In addition, R_2 and R_4 construct a VD to provide BV for Q_6, which remains turned on. This is the second process section (green dotted lines in Figure 3). Therefore, the invert rectifier circuit performs rapid switching of states.

(3) Mode 3: According to Figures 4 and 6, t_4–t_7 are the off time of Q_5 (i.e., Q_{5off} time), and t_5 and t_6 are the on time of Q_6 (i.e., Q_{6on} time). In other words, when u_{ba} increases from u_d = Uth to the peak and then decreases to u_d = Uth, Q_6 turns on while Q_5 is blocked. The path of the current has two current loops: power and control loops (red dotted lines in Figure 4). The power loop is from L_2, point b, D_3, and R_L to point *o*, while the control loop is from L_2, point b, R_2, point d, and R_4 to point *o*. Note that point o, Q_6, point a, and the right side of C_2 have the same voltage (0 V) (green dotted lines in Figure 4). Moreover, R_1 and R_3 construct a VD to provide BV for Q_5. Similarly, R_2 and R_4 construct a VD to provide BV for Q_6. In this mode, Q_6 is turned on because $u_{ba} > u_d >$ Uth. On the contrary, Q_5 is blocked because $u_c = u_a = 0$ v. Therefore, the invert rectifier circuit performs negative half-cycle rectification.

(4) Mode 4: According to Figures 5 and 6, when the frequency sine voltage u_{ba} decreases from u_d = Uth to zero, Q_6 enters the amplification region from the conductive region in the time regions t_6 and t_7. It is then blocked at the time point t_7 and the time regions t_7 and t_{10}. In addition, when Q_6 enters the amplification region and is blocked, the power is quickly released by a circuit loop of R_1 and D_1. This is the first process section (red dotted lines in Figure 5). On the other hand, the voltage is reversed at the next moment. When u_{ab} increases from zero to u_c = Uth, Q_5 enters the amplification region in the time regions t_7 and t_8. It then turns on at the time point t_8 and the time regions t_8 and t_9 when u_{ab} increases and $u_c >$ Uth. In addition, R_1 and R_3 construct a VD to provide BV for Q_5, which remains turned on. This is the second process section (green dotted lines in Figure 5). Therefore, the invert rectifier circuit also performs rapid switching of states.

It can be deduced from the aforementioned analysis that L_2 and C_2 comprise a series resonant tank, whose resonant frequency determines that of the sine voltage on the Rx side. Furthermore, the switching frequency of Q_5 and Q_6 and the rectification frequency of the rectifier diode are determined by the frequency of the sine voltage stimulation on the Rx side. More precisely, the function of automatic FT is performed, where R_1–R_4 play a crucial role. In addition, due to R_1–R_4, the self-excited invert rectifier performs the SD of MOSFETs

during the inversion process without the need for the signal detector and microcontroller that are used in traditional rectifiers. This significantly reduces the complexity of the control and structure as well as the cost, and increases the TE of the WPT system. Furthermore, R_1 and R_3 construct a VD to provide BV for Q_5. Similarly, R_2 and R_4 construct a VD to provide BV for Q_6. Moreover, R_1 and D_1 construct a circuit loop and quickly release power when Q_6 is blocked. Note that R_2 and D_2 have the same function. The two circuit loops provide a quick energy release channel, which accelerates the mode switching and reduces the power loss of Q_5 and Q_6. In addition, the product of Q_5 and Q_6 is AGM035N10A, which obtains 3 mΩ from the drain-source on-state resistor. It can reduce the power loss during the functioning of Q_5 and Q_6. Finally, D_5 and D_6 perform voltage stabilization to protect Q_5 and Q_6.

3. Analysis of the Power Loss of the Self-Excited Invert Rectifier

The circuits of the self-excited invert rectifier can be equivalent according to Figure 7. The circuit model has two resonant circuits, linked magnetically by mutual inductance M. U_S is the input power of the Tx; R_S is the sum of the loss resistor and radiation resistor of the Tx; R_k is the sum of the loss resistor and radiation resistor of the Rx, which mainly includes the working resistors of Q_5, Q_6, D_3, and D_4; L_1 and L_2 are the inductors; C_1 and C_2 are the capacitors; R_L is the load resistor; U_L is the load voltage; and $\dot{I}_1$ and $\dot{I}_2$ are the currents of the Tx and Rx loops, respectively.

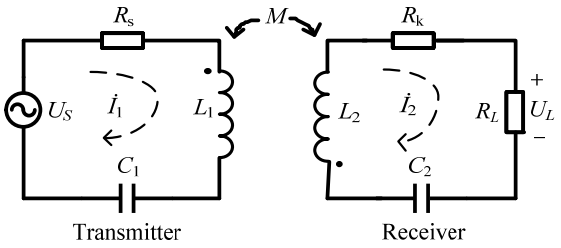


Figure 7. Equivalent circuit of the WPT system with self-excited invert rectifier.

According to Figure 7, Kirchhoff's voltage law, and angular frequency ω, the WPT system with the self-excited invert rectifier can be expressed as

$$\begin{cases} U_S = Z_1\dot{I}_1 - j\omega M\dot{I}_2 \\ 0 = Z_2\dot{I}_2 - j\omega M\dot{I}_1 \end{cases} \tag{1}$$

The self-impedance values Z_1 and Z_2 are given by

$$\begin{cases} Z_1 = R_S + j\omega L_1 + \frac{1}{j\omega C_1} \\ Z_2 = R_k + R_L + j\omega L_2 + \frac{1}{j\omega C_2} \end{cases} \tag{2}$$

The output power (OP) P_{out} can be given as [6]

$$P_{out} = |\dot{I}_2|^2 \ R_L = \frac{\sigma\beta\tau^2(1+\xi^2)}{\sigma^2(1+\xi^2+\tau^2)^2 + \xi^2(1+\xi^2-\sigma\tau^2)^2}\frac{{U_S}^2}{R} \tag{3}$$

where $\sigma = R_S/(R_k + R_L)$ and $\beta = R_L/(R_k + R_L)$ are the resistor ratios, $R = R_k + R_L$ is the resistor of the Rx side, $\tau = \omega M/(R_S(R_k + R_L))^{0.5}$ is the impedance-coupled factor, and ξ is the frequency-detuning factor.

The TE η can be written as [6]

$$\eta = \frac{P_{out}}{P_{in}} = \frac{\left|\dot{I}_2\right|^2 R_L}{\left|\dot{I}_1\right|_2 R_s + \left|\dot{I}_2\right|^2 (R_k + R_L)} = \frac{\beta\tau^2}{1 + \xi^2 + \tau^2} \quad (4)$$

According to Equation (3), $\sigma = R_S/(R_k + R_L)$, $\beta = R_L/(R_k + R_L)$, and $R = R_k + R_L$; when R_S and R_k decrease, the OP P_{out} increases. According to Equation (4), $\beta = R_L/(R_k + R_L)$, and $\tau = \omega M/(R_S(R_k + R_L))^{0.5}$; when R_S and R_k decrease, and $\xi = 0$, the TE η increases.

In summary, when R_S and R_k decrease, the OP and TE improve. On the Rx side, the self-excited invert rectifier could reduce the value of R_k by decreasing the power losses of the MOSFETs (Q_5 and Q_6) and the forward voltage losses of the rectifier diodes (D_3 and D_4).

4. Experimental Results

Figure 8 shows an experimental block diagram of the WPT system that includes a self-excited invert rectifier, where R_S is the sum of the loss and radiation resistors of the Tx; R_k is the sum of the loss and radiation resistors of the Rx, which mainly includes the working resistors of Q_5, Q_6, D_3 and D_4; C_3 is the filter capacitor; U_L is the DC voltage of the load; and R_L is the load resistor. Table 2 presents the parameters of the self-excited invert rectifier experimental equipment.

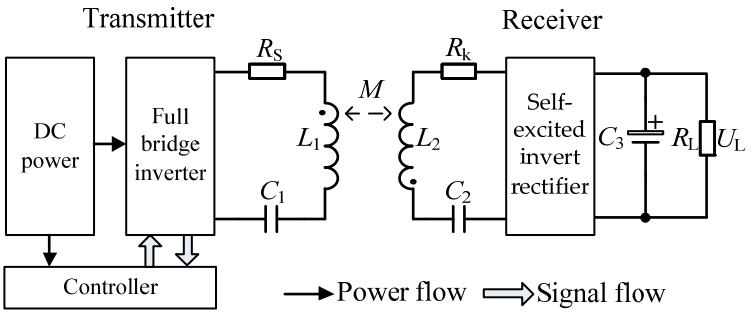


Figure 8. Block diagram of the WPT system that includes a self-excited invert rectifier.

Table 2. Parameters of the self-excited invert rectifier experimental equipment.

Parameter	Tx	Rx
Natural frequency f_0/kHz	81.3	81.3
Inductance L/μH	15.0	15.0
Capacitor C/nF	294.6	294.6
Inside diameter of the coil φ/mm	150	150
Outside diameter of the coil Φ/mm	180	180
Layers of the coil	1	1
Number of turns n	5	5
Coupling distance/mm	0–40	
TE	<91.4%	
Load R_L/Ω	Lamp 20	
Input voltage/V Vdc	36	
Input power/W	200	

Figure 9 shows a self-excited invert rectifier experimental equipment able to perform the SD and SS of the MOSFETs. It has a wireless power transfer capacity of 200 W. It mainly includes a TH2827A bridge analyzer (Tonghui, Changzhou, China), a TMi120S infrared thermal imaging instrument (UNI-T, Dongguan, China), a P6022 current probe (Tektronix, Beaverton, OR, USA), and a DS1054 digital oscilloscope (RIGOL, Suzhou, China).

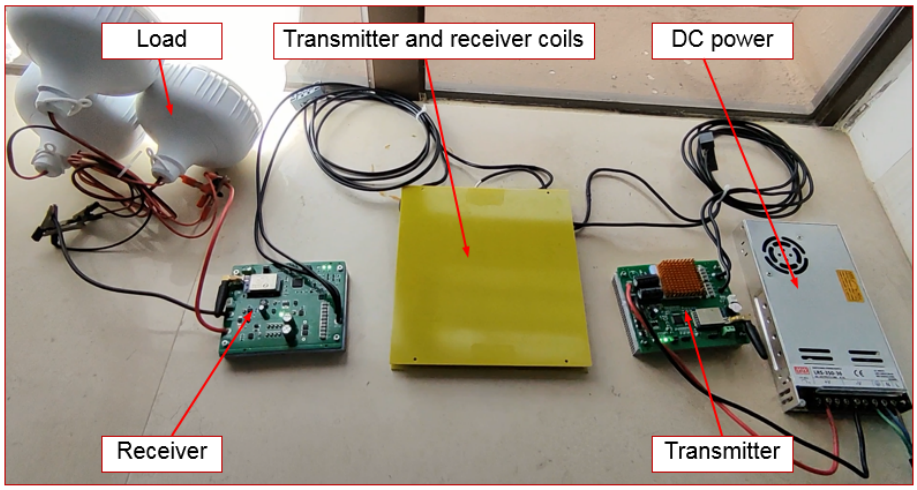


Figure 9. A self-excited invert rectifier experimental equipment able to perform the SD and SS of the MOSFETs.

(1) Experimental verification of the self-excited invert rectification method

Based on the aforementioned theory results, L_2 and C_2 comprise a series resonant tank, whose frequency determines that of the sine voltage at the Rx side. Furthermore, the switching frequency of Q_5 and Q_6 and the rectification frequency of the rectifier diode are determined by the frequency of the sine voltage stimulation on the Rx side. In Figures 10 and 11, the working frequency of the self-excited invert rectifier is 75.7 kHz. Since the working frequency of the Tx is 75.7 kHz, the self-excited invert rectifier performs the FT. It can then be deduced that the self-excited invert rectifier can perform the SD and SS of the MOSFETs without a microcontroller, which greatly simplifies the structure of the invert rectifier.

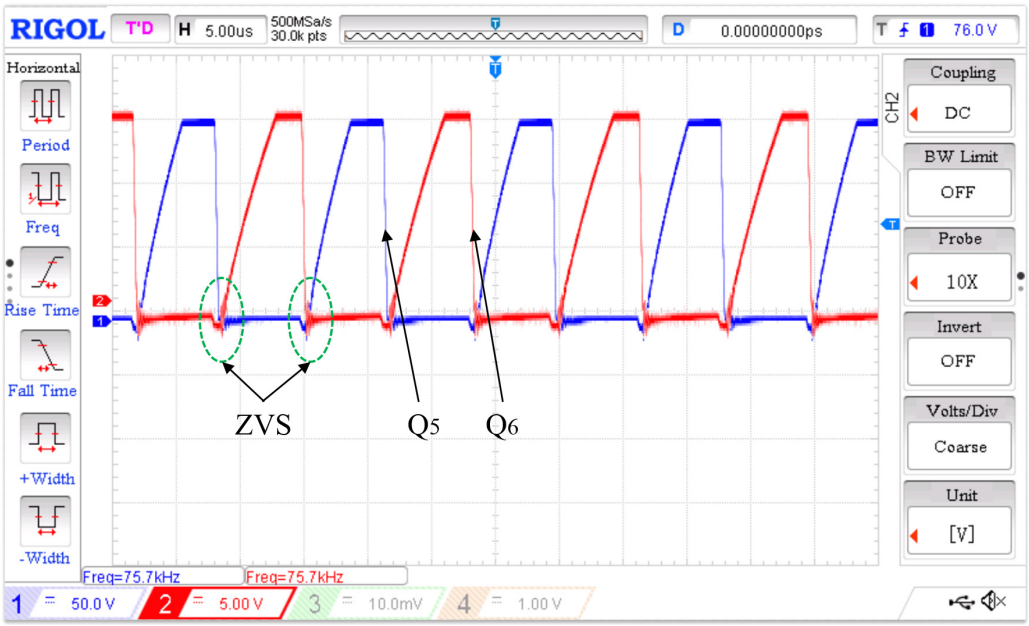


Figure 10. Gate drive waveform (gate−source voltage) of the Q_5 and Q_6 switching tubes.

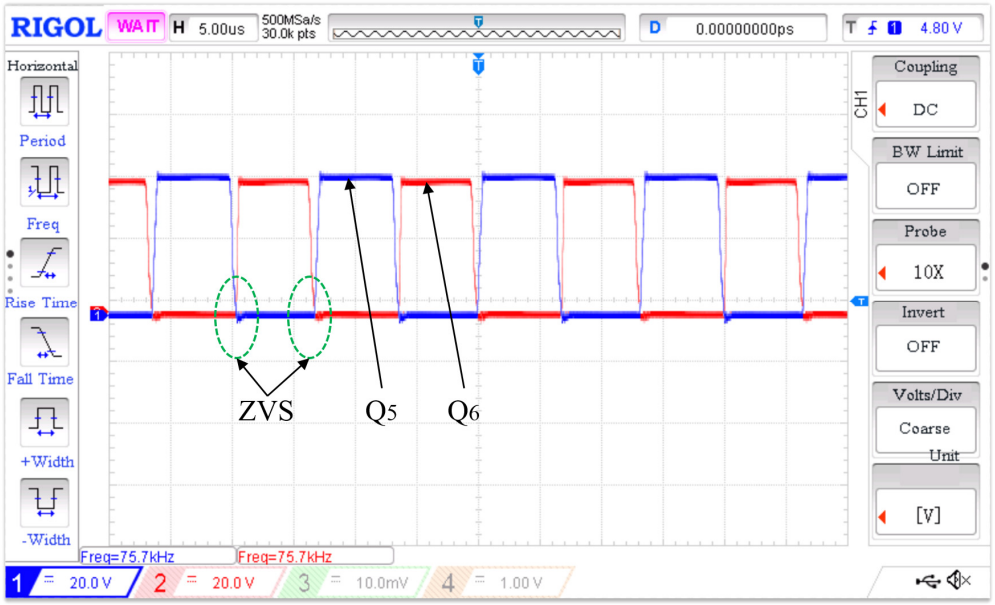


Figure 11. Working waveform (drain−source voltage) of the Q_5 and Q_6 switching tubes.

In Figure 10, the time delay of the gate drive waveform between the Q_5 and Q_6 switching tubes is 220 ns. In Figure 11, the time delay of the working waveform between Q_5 and Q_6 is also 220 ns. This indicates that they are alternately turned on, which ensures the safe and reliable rectification of the self-excited invert rectifier. More precisely, the function of the zero-voltage switch (ZVS) is achieved in the self-excited invert rectifier using D_1 and D_2, R_1 and R_3, and R_2 and R_4. Thus, the invert rectifier circuit performs rapid and reliable switching between Q_5 and Q_6.

In summary, the experimental results are consistent with those of the theoretical analysis of Section 2. They show that the self-excited inverter rectification method is effective.

(2) Experiment for reducing the power loss of the self-excited invert rectifier

According to the aforementioned theory results, R_1–R_4 resistors, Q_5 and Q_6, and D_3 and D_4 are affected by the power loss of the self-excited invert rectifier. This also affects the TE. Thus, key component parameters of the self-excited invert rectifier are required to increase the performance of the self-excited invert rectifier. The key component parameters are shown in Table 3.

Table 3. Key component parameters of the self-excited invert rectifier.

Parameters	Values
R_1–R_4	R_3 = R_4 = 10 kΩ, R_1 = R_2 = 560 Ω, 1 kΩ, 2 kΩ
Q_5 and Q_6	AGM035N10A (drain-source on-state resistor: 3 mΩ, 112 A, 100 V), BSC0702LS (2.3 mΩ, 100 A, 60 V), APG011N04G (0.9 mΩ, 200 A, 40 V)
D_3 and D_4	Silicon carbide Schottky diode: FFSM0865B (Vf = 1.39 V@8 A, 650 V). Schottky barrier rectifiers: SB10100L (Vf: 670 mV@10 A, 100 V), SB1060L (Vf: 550 mV@10 A, 60 V), ST10100L (Vf: 590 mV@10 A, 100 V)

R_1 with R_3 and R_2 with R_4 first construct two VDs to provide BVs for Q_5 and Q_6, respectively. R_1 and R_2 should have a suitable value, which allows us to obtain a suitable current to drive Q_5 and Q_6 (e.g., 1 kΩ in Table 3). Thus, high R_1 and R_2 values do not have

sufficient current to drive Q_5 and Q_6 (e.g., 2 kΩ in Table 3). On the other hand, lower R_1 and R_2 values lead to circuit damage due to the excessive carried current (e.g., 560 Ω in Table 3).

In addition, R_1 and D_1 construct a circuit loop and quickly release power when Q_6 is blocked. Note that R_2 and D_2 have the same function. The two circuit loops provide a quick energy release channel, which accelerates the mode switching and reduces the power loss of Q_5 and Q_6.

Moreover, a smaller drain-source on-state resistor of Q_5 and Q_6 results in a smaller power loss. In Table 3, the drain-source on-state resistor of APG011N04G is 0.9 mΩ, and its power loss is smaller than that of other components (e.g., AGM035N10A, BSC0702LS). However, the drain-source voltage should also be taken into consideration to be adapted to the WPT system. In this study, AGM035N10A was used to design the WPT experimental equipment.

Finally, a forward voltage of D_3 and D_4 results in a smaller power loss. In Table 3, the forward voltage of SB1060L is 550 mV, and its power loss is smaller than that of other components (e.g., FFSM0865B, SB10100L, and ST10100L). However, the forward voltage of FFSM0865B is 1.39 V, which is higher than that of other components. FFSM0865B was selected to design the WPT experimental equipment. When it functions, the temperature rapidly increases and the WPT experimental system is damaged. Additionally, the reverse voltage should also be taken into consideration in a WPT system. In this study, ST10100L was finally chosen due to its small forward voltage (590 mV) and higher reverse voltage (100 V).

In Figure 12a, D_3 and Q_5 are on the front of the circuit board. However, D_4 and Q_6 are on the back. Because these two sets of components are symmetrically arranged on the front and back of the circuit board, they should have the same thermal image. Figure 12b shows the thermal image of the front of the circuit board. Several conducted measurements show that the temperatures of D_3 and Q_5 are lower than 34.3 °C. This indicates that the self-excited invert rectifier has higher performance when adopting the aforementioned key component parameters.

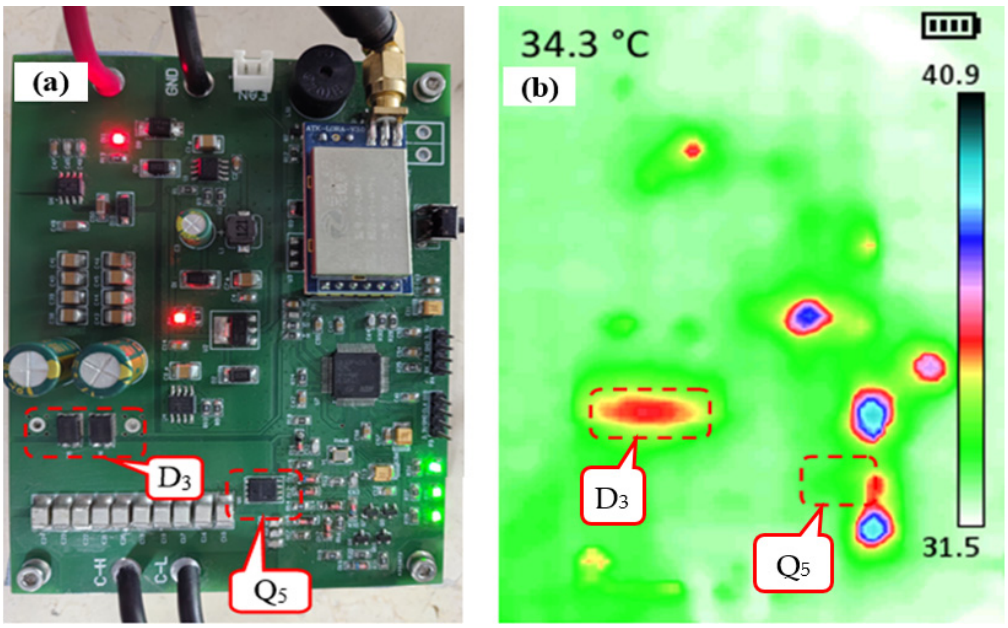


Figure 12. (**a**) Circuit of the Rx and (**b**) temperature image of the self-excited invert rectifier.

In addition, the impact of temperature variation and load resistance needs to be considered in a WPT system. The power loss of the self-excited invert rectifier is low when the system works at an industrial-grade temperature. Moreover, appropriate load resistance is beneficial for improving TE.

In summary, the experimental results for reducing the power loss are consistent with the theoretical analysis of Section 3. It shows that the measures for reducing the power loss of the self-excited invert rectifier are effective.

(3) Experiment for increasing the TE of the self-excited invert rectifier

According to the aforementioned optimizing results of the key component parameters, in Figures 13 and 14, the OP P_1 and TE η_1 are obtained using the full-bridge inverter rectifier of the Rx. On the other hand, the OP P_2 and TE η_2 are obtained using the self-excited invert rectifier of the Rx. Due to the selection of suitable key component parameters for the self-excited invert rectifier, the OP of the WPT system with the self-excited invert rectifier is improved by more than 10 W. Similarly, the TE with the self-excited invert rectifier is increased by more than 5%. More precisely, it reaches 86.2%, while it is only 91.4% in the case of only optimizing the Rx side.

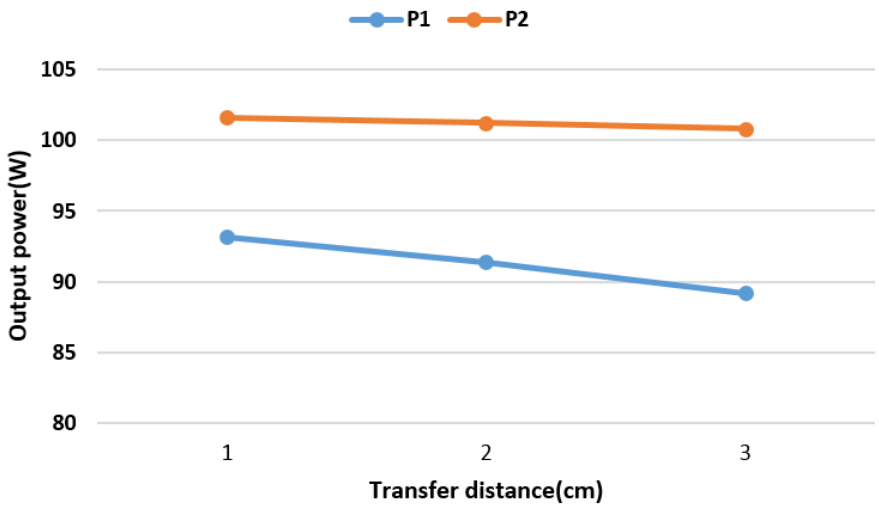


Figure 13. OP of the system as a function of the distance.

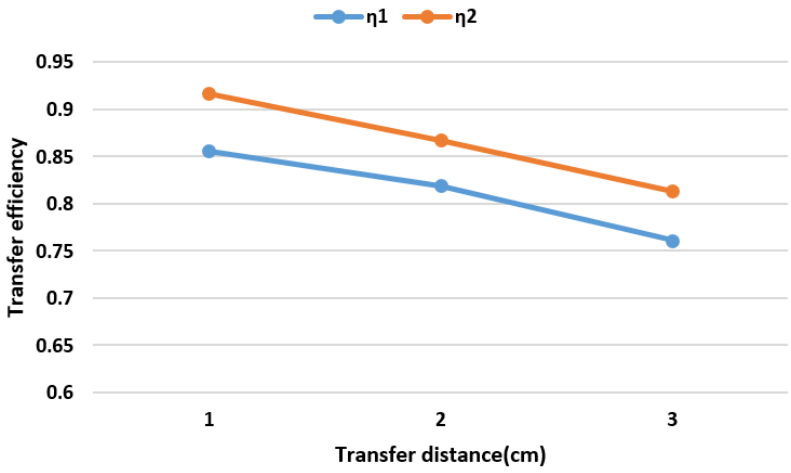


Figure 14. TE of the system as a function of the distance.

According to the aforementioned results of the key component parameters, the OP P_2 and TE η_2 are obtained at different frequencies, which are shown in Figures 15 and 16. It can be seen that, for a transfer distance of 3 cm, the high and flat OP P_2 peaks are reached around 75.7 kHz. For a transfer distance of 1 cm, the peaks of the OP P_2 occur at 61 kHz and 91 kHz, respectively. Additionally, for a transfer distance of 2 cm, the peaks of the OP P_2 occur at 66 kHz and 86 kHz, respectively. Thus, the frequency splitting of the OP occurs at transfer distances of 1 cm and 2 cm [3,21]. However, the high and flat TE η_2 peaks are reached at around 75.7 kHz. The value of the TE η_2 is increased as the transfer distance decreases. According to the aforementioned analysis results, it can be concluded that the optimization of TE is needed to consider the impact of frequency splitting. Thus, in the self-excited invert rectifier experimental equipment, the working frequency of the Tx side is adaptively changed to obtain the maximum value of the TE when the transfer distance changes.

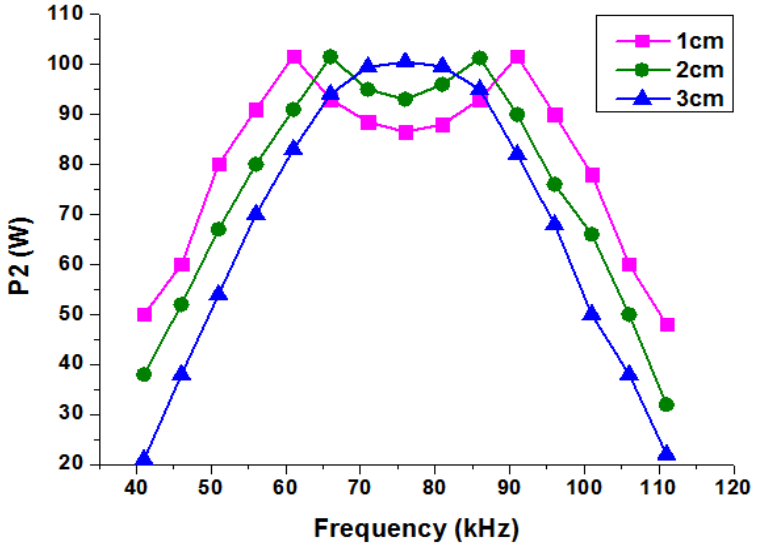


Figure 15. OP P_2 of the system as a function of the frequency.

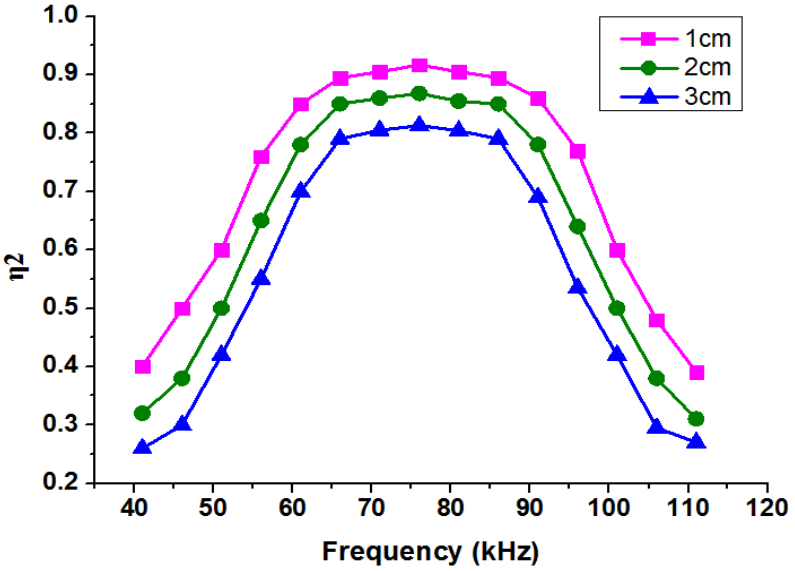


Figure 16. TE η_2 of the system as a function of the frequency.

In summary, the experimental results are consistent with those of the theoretical analysis. They show that the self-excited inverter rectification method is effective. In addition, the self-excited invert rectifier can perform the SD and SS of the MOSFETs as well as the FT function without a microcontroller. This method provides a practical solution for reducing the complexity of the rectifier. It can be clearly seen that the TE is increased using the self-excited invert rectifier and the optimized key component parameters.

5. Conclusions

In this paper, a novel self-excited invert rectification method was proposed to design the invert rectifier of the Rx. This self-excited invert rectifier can perform the SD and SS of the MOSFETs as well as the FT function without a microcontroller. In addition, the TE of the WPT system with the self-excited invert rectifier and optimized key component parameters is increased by more than 5%. Finally, the self-excited invert rectifier of the Rx provides a practical solution for reducing the complexity of the WPT system.

Author Contributions: S.L.: conceptualization, methodology, software, validation, writing—original draft preparation. X.Y.: data curation. G.W.: writing—review and editing. Y.L.: writing—review and editing. All authors have read and agreed to the published version of the manuscript.

Funding: The work was supported by the Guangxi Natural Science Foundation (Grant Nos. 2022GXNSFAA035590 and 2021GXNSFBA196051) and the High Level Talent Foundation Project of Guilin University of Electronic Technology (UF20008Y).

Data Availability Statement: The original contributions presented in this study are included in the article. Further inquiries can be directed to the corresponding author.

Conflicts of Interest: The authors declare no conflicts of interest. The founding sponsors had no role in the design of the study or in the decision to publish the results.

References

1. Tesla, N. Electrical Energy. U.S. Patent 1,119,732, 1 December 1914.
2. Kurs, A.; Karalis, A.; Moffatt, R.; Joannopoulos, J.D.; Fisher, P.; Soljacic, M. Wireless Power Transfer via Strongly Coupled Magnetic Resonances. *Science* **2007**, *317*, 83–86. [CrossRef]
3. Sample, A.P.; Meyer, D.T.; Smith, J.R. Analysis, Experimental Results, and Range Adaptation of Magnetically Coupled Resonators for Wireless Power Transfer. *IEEE Trans. Ind. Electron.* **2011**, *58*, 544–554. [CrossRef]
4. Qin, R.; Li, J.; Sun, J.; Costinett, D. Shielding Design for High-Frequency Wireless Power Transfer System for EV Charging With Self-Resonant Coils. *IEEE Trans. Power Electron.* **2023**, *38*, 7900–7909. [CrossRef]
5. Liu, S.; Yan, X.; Xu, G.; Wang, G.; Liu, Y. An Eight-Coil Wireless Power Transfer Method for Improving the Coupling Tolerance Based on Uniform Magnetic Field. *Processes* **2024**, *12*, 2109. [CrossRef]
6. Liu, S.; Liu, Y. Transfer characteristics of the MCR-WPT system using two series transmitting coils. *Circuit World* **2019**, *46*, 48–54. [CrossRef]
7. Tang, J.; Na, T.; Zhang, Q. A Novel Full-Bridge Step Density Modulation for Wireless Power Transfer Systems. *IEEE Trans. Power Electron.* **2023**, *38*, 41–45. [CrossRef]
8. Yang, Y. A Passive Augmented Circuit for EMI Reductions of Full-Bridge Inverters With Conventional Phase Shift Control in Wireless Power Transfer Systems. *IEEE Trans. Power Electron.* **2023**, *38*, 13286–13297. [CrossRef]
9. Kavimandan, U.D.; Galigekere, V.P.; Ozpineci, B.; Onar, O.; Mahajan, S.M. The Impact of Inverter Dead-Time in Single-Phase Wireless Power Transfer Systems. *IEEE Trans. Power Electron.* **2022**, *37*, 1074–1089. [CrossRef]
10. Xiong, W.; Yu, Q.; Liu, Z.; Zhu, Q.; Su, M.; Zhao, L.; Hu, A.P. A Dual-Frequency-Detuning Method for Improving the Coupling Tolerance of Wireless Power Transfer. *IEEE Trans. Power Electron.* **2023**, *38*, 6923–6928. [CrossRef]
11. Li, K.; Tan, S.-C.; Hui, R. Dynamic Response and Stability Margin Improvement of Wireless Power Receiver Systems via Right-Half-Plane Zero Elimination. *IEEE Trans. Power Electron.* **2021**, *36*, 11196–11207. [CrossRef]
12. Liu, J.; Xu, F.; Sun, C.; Loo, K.H. A Soft-Switched Power-Factor-Corrected Single-Phase Bidirectional AC–DC Wireless Power Transfer Converter with an Integrated Power Stage. *IEEE Trans. Power Electron.* **2022**, *37*, 10029–10044. [CrossRef]

13. Liu, X.; Wang, Y.; Chen, H.; Mai, J.; Xu, D. A Bidirectional WPT System Using Double-sided LCC Compensation Topology and Full-bridge Active Rectifier. In Proceedings of the 2022 IEEE Transportation Electrification Conference and Expo, Asia-Pacific (ITEC Asia-Pacific), Haining, China, 28–31 October 2022; pp. 1–7.
14. Wu, X.; Yan, H.; Xiao, J.; Chen, S.; Wu, N.; Mo, Y. Analysis of Phase-Shifting Constant Voltage Control of LCC-S Wireless Power Transfer System. In Proceedings of the 2023 International Conference on Electronics and Devices, Computational Science (ICEDCS), Marseille, France, 22–24 September 2023; pp. 54–58.
15. Wu, W.; Luo, D.; Hong, J.; Tang, Z.; Chen, W. A Six-Switch Mode Decoupled Wireless Power Transfer System with Dynamic Parameter Self-Adaption. *Electronics* **2023**, *12*, 2314. [CrossRef]
16. Wang, Y.; Liu, W.; Huangfu, Y. A Wireless Power Transfer System with Robust Primary-Sided Current Based on the Self-Excited Inverter. In Proceedings of the 2019 IEEE International Conference on Industrial Technology (ICIT), Melbourne, VIC, Australia, 13–15 February 2019.
17. Yao, W.; Weiguo, L.; Yigeng, H.; Yuntian, L. Wireless Power Transfer System Based on the Self-Excited Inverter. *Trans. China Electrotech. Soc.* **2019**, *34*, 4751–4760.
18. Zhao, Z.; Luo, B.; Tan, T.; Wang, C.; Sun, Z. Improved Self-Excited Resonant Wireless Power Transmission System. *J. Shanghai Jiao Tong Univ.* **2023**, *57*, 859–867.
19. Yang, J.; Chen, W.; Xie, W. Research on Wireless Power Transmission System Based on Self-excited Push-pull Oscillator. *J. Power Supply* **2021**, *19*, 142–152.
20. Zhang, X.; Yuan, Z.; Yan, Q.; Wei, B.; Wang, S. Analysis of the Magnetic Shielding Characteristics of Magnetic Coupling Resonant Wireless Power Transmission System Based on Self-excited Push-pull Converter. *Proc. CSEE* **2018**, *38*, 555–561+686.
21. Liu, S.; Tan, J.; Wen, X. Research on the Impedance Characteristic of a Two-Coil Wireless Power Transfer System. *IEICE Trans. Electron.* **2018**, *101*, 711–717. [CrossRef]

Disclaimer/Publisher's Note: The statements, opinions and data contained in all publications are solely those of the individual author(s) and contributor(s) and not of MDPI and/or the editor(s). MDPI and/or the editor(s) disclaim responsibility for any injury to people or property resulting from any ideas, methods, instructions or products referred to in the content.